EPTT 2024
Escola de Primavera de Transição e Turbulência

ABCM
Associação Brasileira de Engenharia e Ciências Mecânicas

EPTT-2024-XXXX
TURBULENCE MODELING IN NONPREMIXED SOOTING FLAMES: ENTRAINMENT EFFECTS AND IMPLICATIONS

Fabio Henrique Bastiani
Pedro Bianchi Neto
Dirceu Noriler
Universidade Estadual de Campinas, Chemical Engineering School - Albert Einstein 500, Campinas, Brazil
f264197@dac.unicamp.br, p228092@dac.unicamp.br, dnoriler@unicamp.br

Abstract. *Turbulence modeling is a crucial area in fluid dynamics and combustion engineering, where the interplay between turbulent flows and chemical reactions dictates the efficiency and emissions of combustion systems. Accurate predictions of these processes are essential for developing cleaner and more efficient combustion technologies. Turbulence is a complex phenomena that presents a significant challenges to fully resolve, necessitating the development of robust modeling techniques or effective approximations. This paper investigates the impact of different turbulence models on temperature and soot volume fraction predictions in non-premixed ethylene-air flames. The $k-\varepsilon$ standard, $k-\varepsilon$ realizable, and $k-\omega$ Shear-Stress Transport (SST) models are employed to close the RANS equations. Analyses in cold gas simulations reveal that entrainment may be overpredicted by the standard $k-\varepsilon$ and $k-\omega$ SST models. Results indicate that the choice of turbulence model significantly affects flame structure and soot formation, with the $k-\varepsilon$ realizable model providing accurate predictions of flame temperature and soot volume fraction in agreement with experimental data. This study contributes to the ongoing effort to enhance cost-effective turbulence modeling, offering insights into model strengths and limitations in non-premixed turbulent flames.*

Keywords: *turbulence modeling, non-premixed flames, soot formation, entrainment, simulation.*

1. INTRODUCTION

Turbulence modeling represents a critical area of research in fluid dynamics and combustion engineering. The complex interplay between turbulent flows and chemical reactions governs the efficiency and emissions of combustion systems, making it a vital topic for both academic investigation and industrial application. Understanding and accurately predicting these processes are essential for the development of cleaner and more efficient combustion technologies. Turbulence remains one of the unresolved problems of physics, and its modeling has evolved over the years (Pope, 2000; De *et al.*, 2018; Turutoglu and Cadirci, 2023).

Turbulence, characterized by stochastic properties, significantly enhances the mixing of fuel and oxidizer in engines and chemical reactors, thereby affecting the combustion process. Turbulence in combustion involves addressing the interaction between turbulent eddies and the flame structure, which directly affects flame stability, heat release, and pollutant formation (Magnussen and Hjertager, 1977; De *et al.*, 2018). Common approaches to turbulence modeling include Reynolds-Averaged Navier-Stokes (RANS) equations, Large Eddy Simulation (LES), and Direct Numerical Simulation (DNS), each offering different levels of accuracy and computational cost (Pope, 2000). LES resolves larger scales of turbulence while modeling smaller scales, providing good accuracy with manageable computational cost. DNS, on the other hand, resolves all scales of turbulence, remaining computationally prohibitive for practical engineering applications. RANS models represent a compromise between accuracy and computational efficiency, relying on averaged quantities to predict the flow field (Launder and Spalding, 1974; Magnussen and Hjertager, 1977; Menter, 1994; Shih *et al.*, 1995; Pope, 2000).

Throughout history, turbulence modeling has been a subject of intense research, with several approaches proposed to address this complex problem. Turbulence is inherently three-dimensional and unsteady, making it challenging to fully resolve. Thus, modeling this phenomenon is fundamental to describing and predicting turbulent fluid flow across various contexts (Pope, 2000). A wide range of turbulence models have been developed to address different flow configurations and turbulence characteristics, each with its own strengths and limitations (Launder and Spalding, 1974; Menter, 1994; De *et al.*, 2018). Zero, one, and two-equation models are the most common approaches to turbulence modeling, each

offering different levels of complexity and accuracy.

The $k-\varepsilon$ model, developed by Launder and Spalding (1974), is one of the most widely used models in engineering applications due to its simplicity and computational efficiency. The $k-\varepsilon$ realizable model, proposed by Shih *et al.* (1995), offers improved predictions for complex flows, including free jets. The $k-\omega$ Shear-Stress Transport (SST) model, developed by Menter (1994), is known for its ability to predict adverse pressure gradient flows and near-wall turbulence, making it suitable for wall-bounded flows (Pope, 2000). The choice of an appropriate turbulence model is essential for combustion simulations, as it directly influences the prediction of flame structure, heat release, and pollutant formation (De *et al.*, 2018; Oldenhof *et al.*, 2011).

In this work, we investigate the influence of different turbulence models on the prediction of temperature and soot volume fraction in a non-premixed ethylene-air flame. The $k-\varepsilon$ standard, $k-\varepsilon$ realizable, and $k-\omega$ SST models are employed to close the RANS system of equations. The analysis is conducted in terms of velocity, entrainment, temperature, and soot formation. Comparisons are made between the models in cold simulations, where the flame is absent, to evaluate the entrainment behavior of the jet. The results show that the choice of turbulence model has a significant impact on flame structure and soot formation, highlighting the importance of accurate turbulence modeling in both cold round free jets and combustion simulations.

2. NUMERICAL METHODS

Ethylene gas is injected into a stagnant gas atmosphere through a tube with a diameter of 4.6 mm, at a mass flow rate of 0.48 g/s, following the experimental setup of Yang *et al.* (2005), where the authors gathered experimental data on temperature and soot-related quantities. Computational Fluid Dynamics (CFD) is employed to discretize the governing equations and solve the flow field and combustion process. The numerical simulations are performed using ANSYS Fluent on a 2-D axisymmetric mesh composed of approximately 72,000 elements. The simulated domain has a height of 1 m and a radius of 1 m, although results are presented only in the central region of the domain (0.3 m radius) for clarity. The Grid Convergence Index (GCI) method is employed, and an acceptable discretization error of 0.02% is estimated for the mesh used.

2.1 Turbulence Modeling

In this work, the simulations are based on the Reynolds-Averaged Navier-Stokes (RANS) equations, which are closed using different turbulence models. The Reynolds decomposition is applied to the Navier-Stokes equations, separating the flow variables into mean and fluctuating components, which are then averaged to obtain the RANS equations. A closure problem arises due to the presence of the Reynolds stresses, which must be calculated using known variables in the flow field (Pope, 2000). The most common way to model these quantities is through the Boussinesq hypothesis, which relates the Reynolds stresses to the mean velocity gradients. The eddy viscosity is then the only unknown variable that must be modeled in order to solve the mean velocity field. This is accomplished through the solution of transport equations that relate turbulence quantities in the flow field to the eddy viscosity. ANSYS Fluent provides multiple methods for solving the Navier-Stokes equations, including various forms for turbulence modeling (Ansys, 2022). In this study, the RANS equations were used without any additional terms or modifications. The $k-\varepsilon$ standard, $k-\varepsilon$ realizable, and $k-\omega$ SST models are employed to predict the turbulent flow field and flame structure of the investigated non-premixed ethylene-air flame.

Equations 1 and 2 represent the standard $k-\varepsilon$ model:

$$\frac{\partial(\rho k)}{\partial t}+\nabla\cdot(\rho k\mathbf{u})=\nabla\cdot\left[(\mu+\frac{\mu_t}{\sigma_k})\nabla k\right]+G_k+G_b-\rho\varepsilon, \tag{1}$$

$$\frac{\partial(\rho \varepsilon)}{\partial t}+\nabla\cdot(\rho \varepsilon\mathbf{u})=\nabla\cdot\left[(\mu+\frac{\mu_t}{\sigma_\varepsilon})\nabla \varepsilon\right]+C_{1\varepsilon}\frac{\varepsilon}{k}G_k-C_{2\varepsilon}\rho\frac{\varepsilon^2}{k}, \tag{2}$$

where k is the turbulent kinetic energy, ε is the turbulent dissipation rate, $\mathbf{u}$ is the velocity vector, μ is the dynamic viscosity, μ_t is the turbulent viscosity, G_k represents the generation of turbulence kinetic energy k due to velocity gradients, G_b is the generation of k due to buoyancy effects. The constants $C_{1\varepsilon}$, $C_{2\varepsilon}$, σ_k, and σ_ε are model-specific constants with standard values $C_{1\varepsilon}=1.44, C_{2\varepsilon}=1.92, \sigma_k=1.0, \sigma_\varepsilon=1.3$.

The realizable $k-\varepsilon$ model addresses the limitations and outcomes of the standard $k-\varepsilon$ model, providing a more accurate prediction of complex flows (Shih *et al.*, 1995). This approach includes a different formulation for calculating the eddy viscosity and a modified transport equation for the dissipation rate (ε) derived from an exact equation for the transport of the mean-square vorticity fluctuation. The transport of turbulent kinetic energy (k) follows Equation 1, while the transport of the turbulent dissipation rate (ε) is given by:

$$\frac{\partial(\rho \varepsilon)}{\partial t}+\nabla\cdot(\rho \varepsilon\mathbf{u})=\nabla\cdot\left[(\mu+\frac{\mu_t}{\sigma_\varepsilon})\nabla \varepsilon\right]+\rho C_1 S\varepsilon-\rho C_2\frac{\varepsilon^2}{k+\sqrt{\nu\varepsilon}}+C_{1\varepsilon}\frac{\varepsilon}{k}, \tag{3}$$

where $C_1 = \max\left[0.43, \frac{\eta}{\eta+5}\right]$, $\eta = S\frac{k}{\varepsilon}$, and $S = \sqrt{2S_{ij}S_{ij}}$. ν is the kinematic viscosity, and S_{ij} is the strain rate tensor. The model constants are slightly different from those in the standard $k-\varepsilon$ model, with $C_{1\varepsilon} = 1.44$, $C_2 = 1.9$, $\sigma_k = 1.0$, and $\sigma_\varepsilon = 1.2$.

The $k-\omega$ SST model combines the $k-\omega$ model for the near-wall region and the $k-\varepsilon$ model for the free stream. The transport equations for k and ω are given by:

$$\frac{\partial(\rho k)}{\partial t} + \nabla\cdot(\rho k\mathbf{u}) = \nabla\cdot\left[(\mu + \frac{\mu_t}{\sigma_k})\nabla k\right] + G_k + G_b - Y_k, \tag{4}$$

$$\frac{\partial(\rho \omega)}{\partial t} + \nabla\cdot(\rho \omega\mathbf{u}) = \nabla\cdot\left[(\mu + \frac{\mu_t}{\sigma_\omega})\nabla \omega\right] + G_\omega + G_{\omega b} + D_\omega - Y_\omega, \tag{5}$$

where G_k and G_ω are the generation terms, G_b and $G_{\omega b}$ are the generation terms due to buoyancy effects, Y_k and Y_ω are the dissipation terms, and D_ω is the cross-diffusion term. The turbulent Prandtl numbers (σ_k, σ_ω) are calculated as:

$$\sigma_k = \frac{1}{F_1/\sigma_{k,1} + (1-F_1)/\sigma_{k,2}}, \tag{6}$$

$$\sigma_\omega = \frac{1}{F_1/\sigma_{\omega,1} + (1-F_1)/\sigma_{\omega,2}}, \tag{7}$$

where F_1 is the blending function, and $\sigma_{k,1}, \sigma_{k,2}, \sigma_{\omega,1}, \sigma_{\omega,2}$ are constants. The function F_1 is defined by

$$F_1 = \tanh(\phi^4) \tag{8}$$

$$\phi = \min\left[\max\left(\frac{\sqrt{k}}{0.09\omega y}, \frac{500}{\rho y^2\omega}\right), \frac{4\rho k}{\sigma_{\omega,2}D_\omega^+ y^2}\right] \tag{9}$$

$$D_\omega^+ = \max\left[2\rho\frac{1}{\sigma_{\omega,2}}\frac{1}{\omega}\nabla k\nabla\omega, 10^{-10}\right] \tag{10}$$

in which y is the distance to the next surface and D_ω^+ is the positive part of the cross-diffusion term (D_ω). The cross-diffusion term appears in the $k-\omega$ SST model due to the blending between the $k-\varepsilon$ and $k-\omega$ formulations. This term arises with the transformation of the ε equation into the ω equation, accounting for the differences in how ε and ω are defined and diffuse. This term allows for smooth transitions within the two approaches, and modify the dissipation rate in regions where neither the pure $k-\varepsilon$ nor the $k-\omega$ models are very accurate. The cross-diffusion term is calculated as:

$$D_\omega = 2(1-F_1)\rho\frac{1}{\sigma_{\omega,2}}\nabla k\nabla\omega \tag{11}$$

The blending function F_1 allows for the interchange between the $k-\omega$ and $k-\varepsilon$ formulations, turning the $k-\omega$ SST model into a robust and accurate formulation of the $k-\omega$ model for the near-wall region and the $k-\varepsilon$ model for the free stream. More details about the generation and dissipation terms can be found in Menter (1994) and Ansys (2022).

2.2 Eddy Viscosity Calculation

In the $k-\varepsilon$ models, equations for k and ε are solved, while in the $k-\omega$ SST model, equations for k and ω are solved. This implies a change in the calculation of the eddy viscosity. Although the turbulence variables are related by $\varepsilon = C_\mu k\omega$, the eddy viscosity is calculated differently for each model. In the $k-\varepsilon$ models, the eddy viscosity is calculated as:

$$\mu_t = \rho C_\mu\frac{k^2}{\varepsilon}, \tag{12}$$

where $C_\mu = 0.09$. The realizable version of the $k-\varepsilon$ model proposed by Shih *et al.* (1995) contains an alternative formulation for the calculation of the eddy viscosity, with the parameter C_μ being expressed as a function of the turbulent kinetic energy and the turbulent dissipation rate. In the $k-\varepsilon$ realizable approach, C_μ is calculated through:

$$C_\mu = \frac{1}{A_0 + A_s\frac{kU^*}{\varepsilon}}, \tag{13}$$

where

$$U^* = \sqrt{S_{ij}S_{ij} + \Omega_{ij}\Omega_{ij}}, \tag{14}$$

where Ω_{ij} is the rotation rate tensor, A_0 is a constant and A_s is also expressed by means of the strain rate tensor (Shih *et al.*, 1995).

The eddy viscosity for the $k-\omega$ SST model is calculated as:

$$\mu_t = \frac{\rho k}{\omega} \frac{1}{\max\left[\frac{1}{\alpha^*}, \frac{SF_2}{a_1\omega}\right]} \tag{15}$$

where S is the strain rate magnitude, α^* is a damping coefficient for low-Re corrections and F_2 is given by:

$$F_2 = \tanh(\phi_2^2) \tag{16}$$

$$\phi_2 = \max\left[\frac{2\sqrt{k}}{0.09\omega y}, \frac{500\mu}{\rho y^2 \omega}\right] \tag{17}$$

2.3 Combustion Modeling

The chemical kinetics of the combustion process are described by the Gri-Mech 3.0 mechanism, which includes 53 species and 325 reactions (Frenklach *et al.*, 1995). Turbulence-chemistry interaction is accounted for using the Eddy Dissipation Concept (EDC) model (Magnussen, 1981), and radiation heat transfer is considered with the P-1 model. The mixture is treated as an ideal gas. Thermal conductivity (k) and viscosity (μ) of the pure species are calculated using kinetic theory, while the mixture properties are determined according to kinetic theory and ideal gas mixture laws. The heat capacity (C_p) of the pure species is calculated using a piecewise polynomial approach (from Gri-Mech 3.0), and the heat capacity of the mixture is obtained through a mass-weighted mixing law. In this study, we employ the soot modeling framework initially proposed by Boulanger *et al.* (2007), which consists of three equations to describe soot formation. This model outlines the process from the initial formation of soot nuclei to the growth of soot particles. The model applied here is a blend of the approaches presented by Tesner *et al.* (1971) and Magnussen and Hjertager (1977). Equation 18 represents the concentration of incipient nuclei particles, Equation 19 explains the formation of soot mass fraction, and Equation 20 serves as a population balance equation for soot particles.

$$\frac{\partial}{\partial t}(\rho n^*) + \nabla\cdot(\rho \mathbf{v} n^*) - \nabla\cdot\left(\frac{\mu_t}{\sigma_t}\nabla n^*\right) = a_0^* \rho_f e^{\left(\frac{-T_a}{T}\right)} + F c_{n^*} - g_0 c_{n^*} c_N - S'_{ox} \tag{18}$$

$$\frac{\partial}{\partial t}(\rho Y_s) + \nabla\cdot(\rho \mathbf{v} Y_s) - \nabla\cdot\left(\frac{\mu_t}{\sigma_t}\nabla Y_s\right) = K_G c_f c_N + a c_a c_n - c_N A_s S_{ox,ns} \tag{19}$$

$$\frac{\partial}{\partial t}(\rho N^*) + \nabla\cdot(\rho \mathbf{v} N^*) - \nabla\cdot\left(\frac{\mu_t}{\sigma_t}\nabla N^*\right) = a c_{n^*} - b c_{N^*} c_{n^*} - K_c\sqrt{T}\left(\frac{\rho Y_s}{\rho_s}\right)^{\frac{1}{6}} c_{N^*}^{\frac{11}{6}} \tag{20}$$

These equations are integrated into the CFD simulations for both flames through the use of User Defined Functions (UDFs). The nano-scale soot particles produced during combustion significantly influence radiation heat transfer within the flame. To determine the soot absorption coefficient, the model proposed in Widmann (2003) is employed, which is then combined with the gas absorption coefficient obtained from the Weighted Sum of Gray Gases model (WSGGM) for the calculation of radiative heat transfer by the P-1 model within the flame. As soot profiles influence temperature of the flame, particle formation and temperature must be analyzed together to properly discuss the results.

3. RESULTS AND DISCUSSION

The results are presented in two sections: cold gas simulations, and combustion and soot formation. The cold gas simulations are performed to evaluate the turbulence models in a simpler scenario, where the flame is absent. The combustion and soot formation simulations are conducted to analyze the influence of turbulence models on flame structure and soot formation in a non-premixed ethylene-air flame.

3.1 Cold Gas Simulations

Velocity contours, with arrowheads indicating flow direction, are depicted in Figure 1. Pure ethylene is injected through a tube with a diameter of 4.6 mm. The flow develops a typical round free jet behavior, where the outer layers of the jet exchange momentum with the stagnant surrounding fluid, decelerating the jet and engulfing surrounding air. The $k-\varepsilon$ realizable model estimates a more stable jet, which seems to drag less air into the injected stream, while the other two models have more similar velocity fields, with a characteristic jet diameter that is larger than for the $k-\varepsilon$ realizable model.

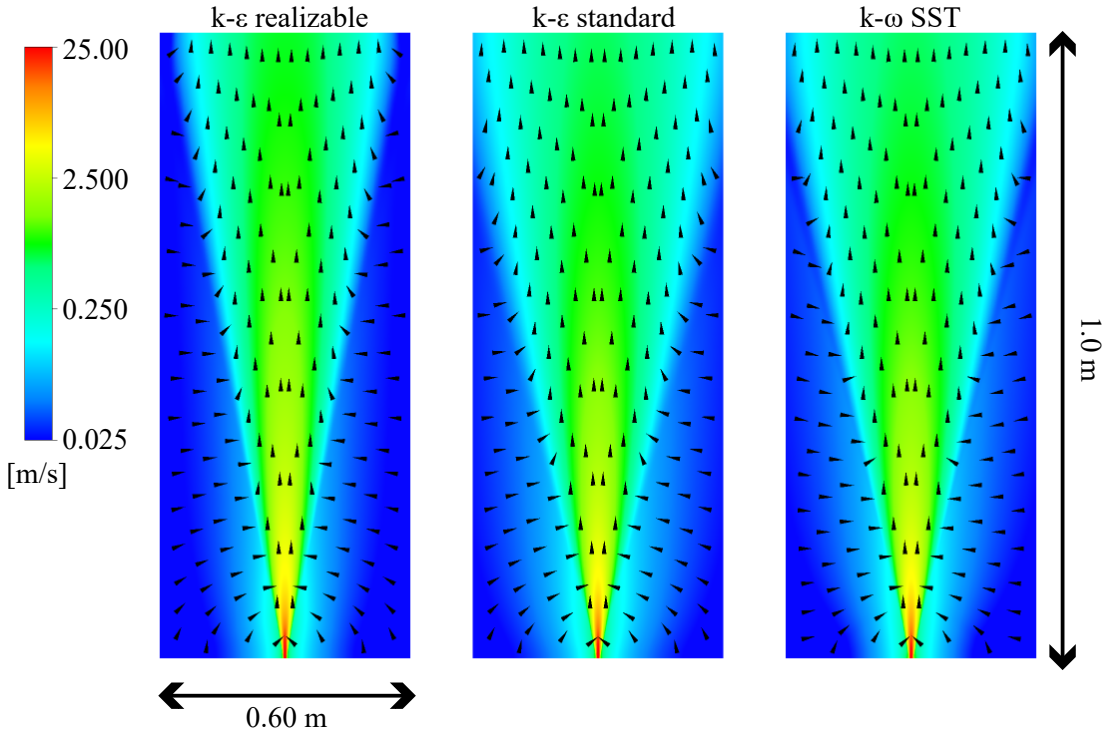

Figure 1. Cold ehtylene-air velocity contours with arrowheads indicating flow direction for the three turbulence models investigated.

In Figure 2, the normalized axial and radial velocity profiles at different heights above the burner are shown. Axially, the $k-\varepsilon$ realizable model estimates slightly higher velocities, while the other two approaches present very similar profiles. Velocity rapidly decays along the centerline due to shear stress between the jet and the stagnant air present in the computational domain. In the radial profiles, the standard $k-\varepsilon$ and $k-\omega$ SST models exhibit very similar velocity decays at all selected heights. The difference in velocity decay between the $k-\varepsilon$ realizable model and the other models increases with the axial distance from the burner, indicating that the $k-\varepsilon$ realizable model predicts a constrained stream, with less momentum being transferred to the surrounding gas. This phenomenon relates to the amount of air drawn into the flame, known as entrainment.

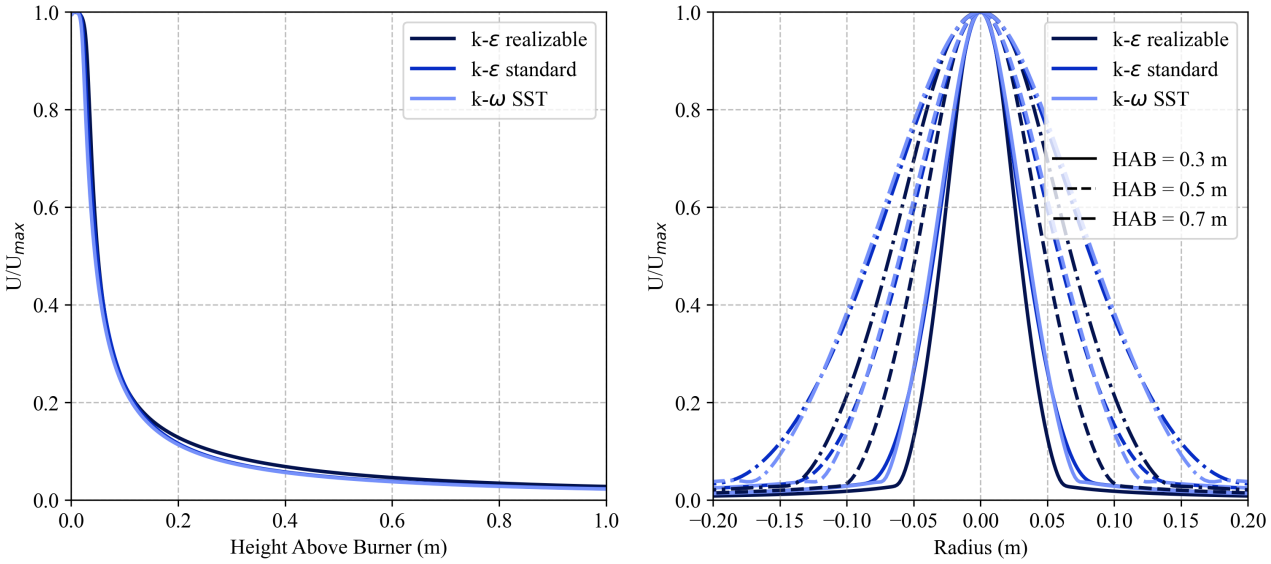

Figure 2. Normalized axial velocity profile along the centerline and normalized radial velocity profiles at different axial positions for the three investigated turbulence models.

Entrainment plays a key role in combustion, as it determines the amount of air drawn into the flame. Therefore, in combustion systems, it is important to have accurate predictions of entrainment to estimate the flame structure correctly

(Cifuentes *et al.*, 2019). In Ricou and Spalding (1961), the authors propose a simple model to predict the entrainment ratio in round jets with good agreement with experiments. The entrainment ratio is defined as a function of the axial distance from the burner and the density ratio between the injected gas and the surrounding fluid:

$$\frac{\dot{m}}{\dot{m}_0} = 0.32 \left(\frac{x}{d_0}\right) \left(\frac{\rho_1}{\rho_0}\right)^{0.5}, \tag{21}$$

where $\dot{m}$ is the mass flow rate of the entrained fluid, $\dot{m}_0$ is the mass flow rate of the jet, x is the axial distance from the burner, d_0 is the diameter of the jet, ρ_1 is the density of the entrained fluid, and ρ_0 is the density of the jet (Ricou and Spalding, 1961). The entrainment ratio is calculated for the three turbulence models and is shown in Figure 3. The $k-\varepsilon$ and $k-\omega$ SST models present similar entrainment ratios, while the $k-\varepsilon$ realizable model shows a lower entrainment ratio at all axial positions, which agrees best with the theoretical model of Ricou and Spalding (1961). From the velocity profiles, we observe that the $k-\varepsilon$ realizable model exhibits a more pronounced peak in the axial direction of the burner and shows a faster decay in the radial direction, indicating less momentum diffusion compared to the other models.

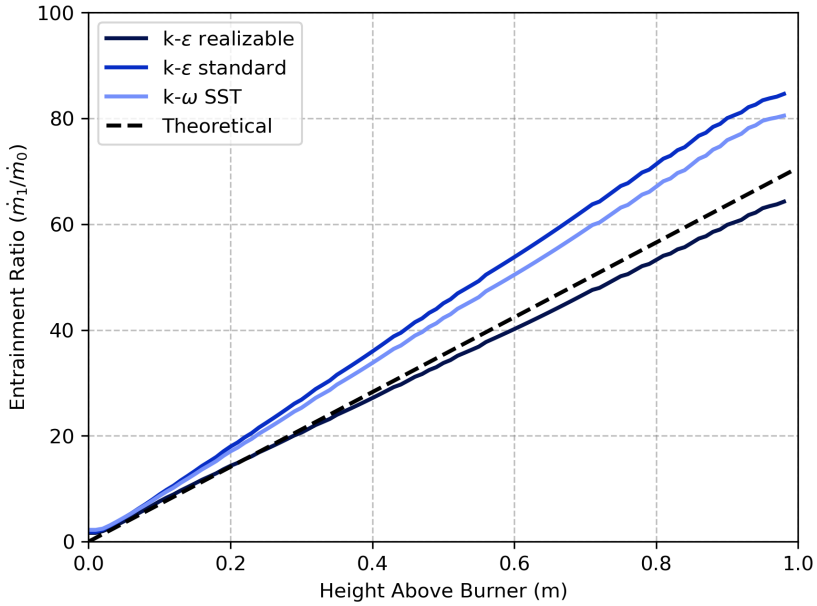

Figure 3. Entrainment ratio along the centerline in the cold gas simulations.

In the work of Kabanshi and Sandberg (2019), the authors discuss how entrainment is influenced by velocity in round free jets. Lower jet velocities result in larger turbulent eddies at the jet boundaries, which draw more air into the flow stream. This phenomenon, known as engulfment, occurs when these large eddies capture the surrounding air and drag it toward the jet's center, thereby enhancing entrainment. As jet velocity increases, the stream's penetration also increases, leading to lower entrainment and reduced momentum loss due to smaller turbulent eddies, which can be observed in the presented models. The main difference between the modeling approaches in this work lies in the calculation of eddy viscosity (μ_t) and the modeling of the turbulent dissipation rate (ε).

Eddy viscosity contours are shown in Figure 4. Arrowheads indicating flow direction are presented to highlight the region where the main jet and the stagnant air are located. The regions separating the main stream and the stagnant gas have high velocity gradients, resulting in large strain magnitudes. The standard $k-\varepsilon$ model estimates a smooth transition of μ_t between the jet and the surrounding air, while the realizable model presents a rapid decay of μ_t in these regions. The $k-\omega$ SST model predicts similar eddy viscosities in the jet core with $k-\varepsilon$ standard but shows an abrupt transition in regions of high velocity gradients. The higher values of μ_t in the standard $k-\varepsilon$ and $k-\omega$ SST models increase momentum diffusion at the outer layers of the jet, thereby increasing the amount of entrainment. The $k-\varepsilon$ realizable model estimates lower values of μ_t in the outer layers of its jet compared to the other models, despite having higher eddy viscosities along the centerline. The decay of μ_t follows the same radial trend as the velocity among the models (Figure 2).

The standard $k-\varepsilon$ model is known for overestimating the eddy viscosity in regions of high strain rate, which may lead to an overestimation of entrainment (Pope, 2000; Versteeg and Malalasekera, 2007). The realizable $k-\varepsilon$ model was developed to address the shortcomings of the standard $k-\varepsilon$ model (Shih *et al.*, 1995). This new formulation allows for a more accurate prediction of eddy viscosity, which is reflected in the calculated entrainment ratio and its proximity to the theoretical values estimated by the model of Ricou and Spalding (1961).

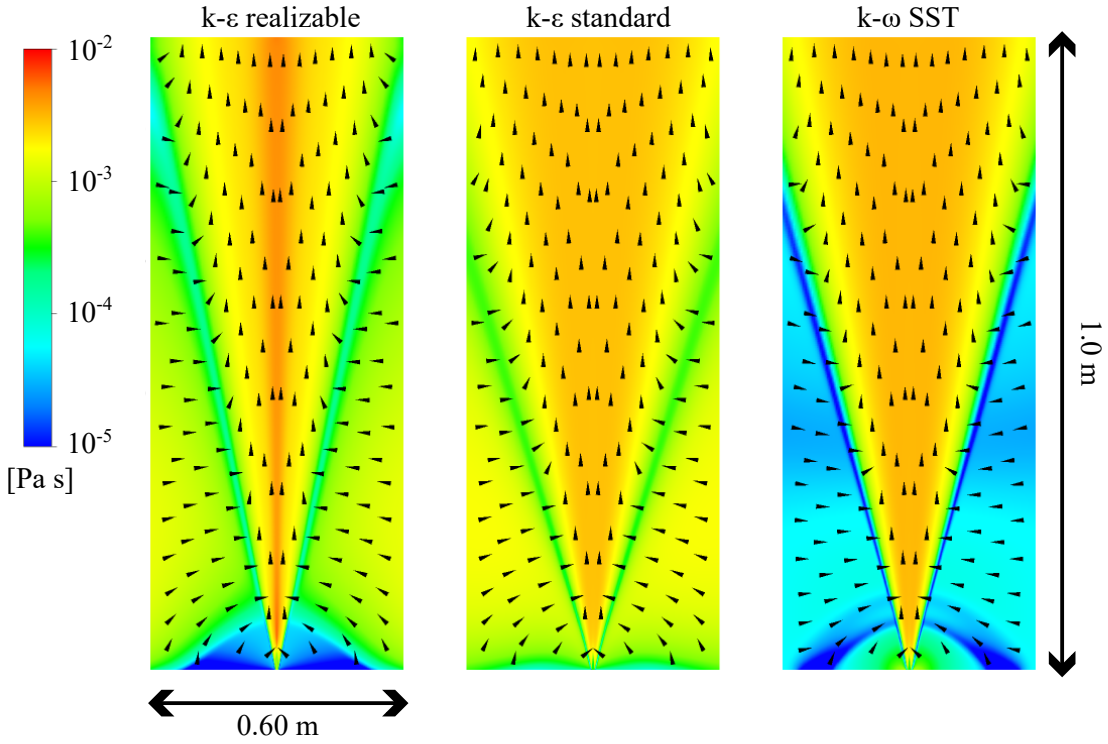

Figure 4. Eddy viscosity contours for the three turbulence models investigated in the cold gas environment.

In the development of the $k-\varepsilon$ realizable model, the authors specifically mention the anomaly in the spread rate of planar and round jets. This issue is addressed by ensuring realizability, i.e., the normal stresses never become negative, which would violate the Schwarz inequality (Shih *et al.*, 1995). In Pope (2000), the author also mentions this deficiency of the standard $k-\varepsilon$ model and asserts that the model constants $C_{\varepsilon 1}$ and $C_{\varepsilon 2}$ could be adjusted to accurately represent the spread rate of specific round jets. Nevertheless, this is not a general solution, as the model constants are not universal and must be adjusted for each specific case. This is evident in Turutoglu and Cadirci (2023) and Marchisio and Barresi (2009), where the authors adjust the $k-\varepsilon$ model constants to achieve better agreement with experiments of round jets. The $k-\varepsilon$ realizable model, on the other hand, is able to predict the spread rate of round jets accurately without the need for adjustments, as the model is inherently realizable and an exact equation for ε is solved.

The $k-\omega$ SST model, which combines the $k-\omega$ model for the near-wall region and the $k-\varepsilon$ model for the free stream, is virtually equivalent to the standard $k-\varepsilon$ approach in this case, as the equations for k and ε are similar. However, in the $k-\omega$ SST model, the model constants are slightly different, and the calculation of eddy viscosity is modified by a factor as described in Equation 15. In the core of the jet, the $k-\varepsilon$ and $k-\omega$ SST models present similar eddy viscosity values. Nevertheless, the eddy viscosity in high shear stress regions changes rapidly in the $k-\omega$ SST model. This is reflected in the entrainment ratio, which is higher than in the $k-\varepsilon$ realizable model but still closer to the theoretical model of Ricou and Spalding (1961) than the standard $k-\varepsilon$ model, ensuring that the modifications made by Menter (1994) also contribute to a better description of round free jets than the standard formulation of the $k-\varepsilon$ model (Launder and Spalding, 1974). The results of the hot gas simulations are presented in the next section, highlighting the influence of turbulence modeling on flame structure and soot formation.

3.2 Combustion and Soot Formation

Temperature contours of the simulated ethylene-air flame are displayed in Figure 5. Qualitatively, the flame structure is similar across all turbulence models, with a well-defined flame front and a region of high temperature at the flame base. The $k-\varepsilon$ realizable model predicts a slightly taller flame[1] (0.75 m), while the standard $k-\varepsilon$ and $k-\omega$ SST models present a more compact flame (0.60 and 0.68 m, respectively). The flame front is more elongated in the $k-\varepsilon$ realizable model, indicating a higher concentration of reactants along the burner axis, while the reactants may diffuse more radially in the other two approaches, as discussed earlier regarding the fundamental differences in turbulence modeling.

Temperature and soot volume fraction profiles for the ethylene-air flame are shown in Figure 6 along the burner axis, with experimental data from Yang *et al.* (2005). Distinctions between the turbulence models used are noticeable. In the temperature profiles, one may observe shifts in the flame front depending on the chosen turbulence model. The turbulence

[1]The flame height is defined as the maximum height where temperature is above 1500 K.

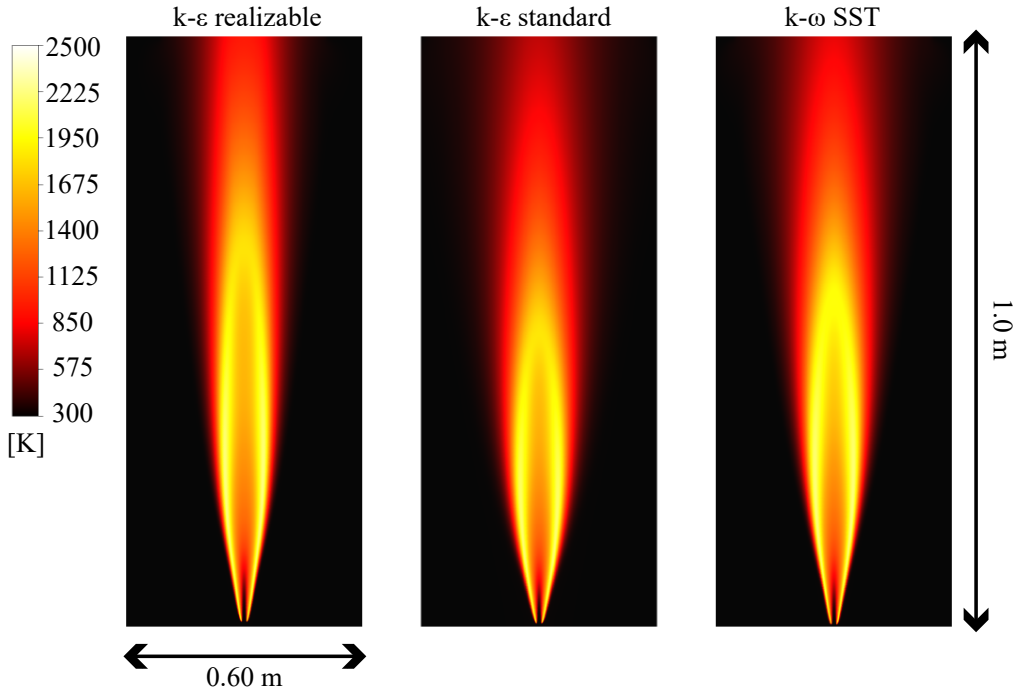

Figure 5. Ethylene-air flame temperature contours for the investigated turbulence models.

models mainly affect how much momentum is lost from the jet to the surroundings. As velocity decreases slightly in the main stream for the standard $k-\varepsilon$ and $k-\omega$ SST models, the chemical species are distributed differently compared to the $k-\varepsilon$ realizable approach, which features a more concentrated jet and less entrained gas. The fuel is injected into a stagnant air atmosphere, reacting with the surrounding air and releasing heat and intermediate soot precursors (C_2H_2). Soot nucleates and grows inside the flame; subsequently, the particles are consumed by oxidation as more oxygen from the surrounding air is supplied to the upper regions of the computational domain.

In the volume fraction profile, the $k-\varepsilon$ realizable model shows good agreement with experiments, while the standard $k-\varepsilon$ model shows early formation and extinction of soot particles. The $k-\omega$ SST model, on the other hand, underpredicts the soot volume fraction in the flame front. This mainly comes down to how temperature and reactant concentrations are distributed along the flame, which ties into earlier discussions on jet velocity and entrainment. Soot formation in this model specifically depends on turbulence kinetic energy (k) and dissipation rate (ε), which influence the oxidation rate of nuclei particles (Magnussen and Hjertager, 1977). Therefore, not only may dislocations occur, but particle dynamics are also affected by the choice of turbulence model.

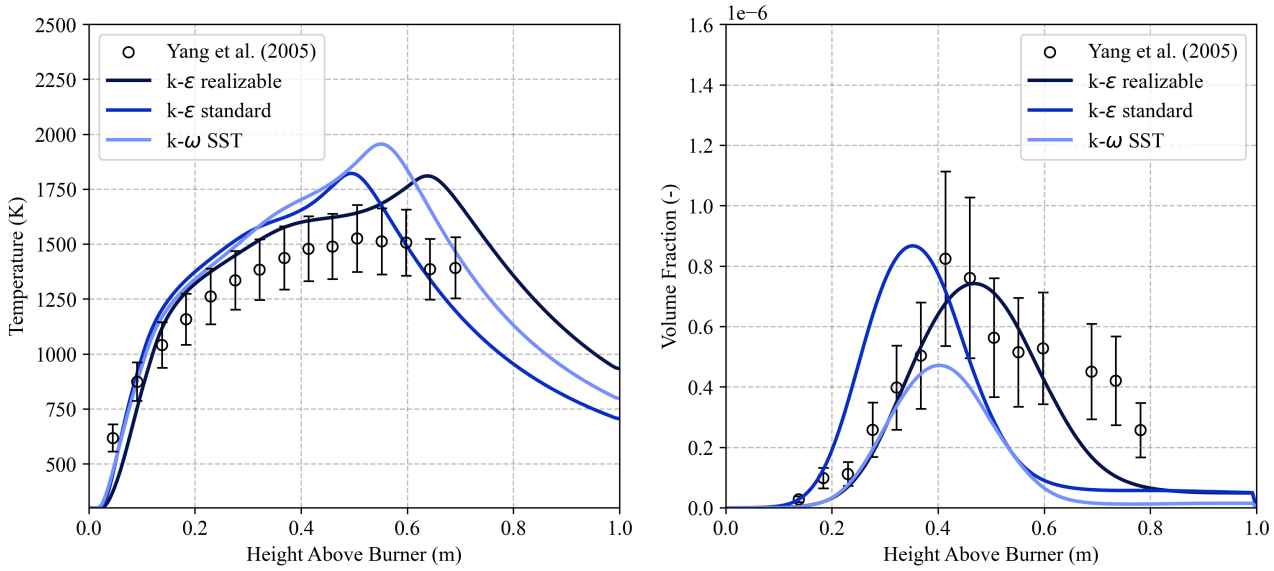

Figure 6. Ethylene-air flame temperature and volume fraction profiles along the centerline for the investigated turbulence models.

As aforementioned, entrainment is influenced by the momentum transferred from the jet to the surrounding fluid; however, in combustion, temperature and density gradients also play a significant role in the entrainment process (Oldenhof *et al.*, 2011). In Figure 7, the entrainment ratios in the hot environment are presented for the three turbulence models investigated. Entrainment increases when compared to cold gas simulations (Figure 3). Within the flame, the hot gas expands, creating a buoyancy effect that further enhances entrainment. As the hot gases rise, they create a low-pressure zone beneath them, which pulls in the surrounding cooler air. This process increases the overall mixing of the gases, enhancing the entrainment of the cooler air into the hot stream. Without the flame, only mechanical forces act to draw surrounding air into the jet; but when the flame is present, more gas is drawn inward due to the combined influence of temperature and drag. Again, one may note that the $k-\varepsilon$ realizable model predicts lower entrainment ratios than the other models, which also means that the characteristic jet cone diameter is smaller, in agreement with the cold gas simulations.

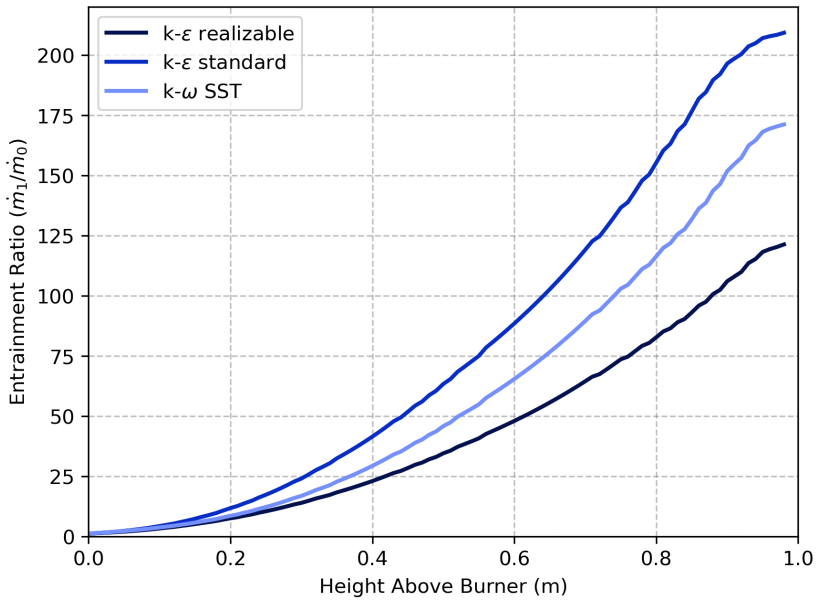

Figure 7. Entrainment ratio along the centerline in the investigated ethylene-air flame.

4. CONCLUSIONS

This work presents simulations of a non-premixed ethylene-air flame and discusses the influence of the $k-\varepsilon$ standard, realizable, and $k-\omega$ SST turbulence models on flame structure and soot formation. The entrainment ratios in the developed round free jet are thoroughly discussed, as they play a vital role in combustion systems. Results of cold gas simulations indicate that the $k-\varepsilon$ realizable model diffuses less momentum to the surrounding gas, resulting in lower entrainment ratios when compared to the other two models. This is supported by the eddy viscosity profiles, which show a more rapid decay of μ_t in regions of high-velocity gradients. The realizable version of the $k-\varepsilon$ model proposes improvements in the calculation of eddy viscosity and the modeling of the turbulent dissipation rate, which allows for a more accurate prediction of entrainment in round free jets. The $k-\varepsilon$ standard model provides poor estimations of entrainment when compared to a validated model from the literature, as well as the $k-\omega$ SST model.

The influence of different turbulence models on flame structure and soot formation is investigated, highlighting the importance of accurate turbulence modeling in combustion simulations. The $k-\varepsilon$ realizable model shows a more elongated flame than the standard $k-\varepsilon$ and $k-\omega$ SST models, resulting in better agreement with experimental temperature data. The $k-\varepsilon$ realizable model also provides more accurate predictions of the soot volume fraction profile. These results indicate that the jet spread rate must be accurately predicted to correctly estimate reactant distribution along the flame and soot formation. Given the high computational cost and complexity of Large Eddy Simulation (LES) and Direct Numerical Simulation (DNS), the use of a simpler turbulence model, such as the $k-\varepsilon$ realizable model, offers a more cost-effective solution while still capturing essential flow characteristics.

5. ACKNOWLEDGEMENTS

This research received support from the São Paulo Research Foundation - FAPESP (2020/08502-9 and 2021/01067-8). This study was financed in part by the Coordenação de Aperfeiçoamento de Pessoal de Nível Superior - Brasil (CAPES) - Finance Code 001. Additional acknowledgements are directed to Conselho Nacional de Desenvolvimento Científico e Tecnológico (CNPq) - Bolsa Produtividade em Desenvolvimento Tecnologia e Extensão Inovadora: 303405/2023-6.

6. REFERENCES

Ansys, 2022. *ANSYS Fluent Theory Guide*. ANSYS Inc., USA.

Boulanger, J., Liu, F., Neill, W.S. and Smallwood, G.J., 2007. "An improved soot formation model for 3d diesel engine simulations". *Journal of Engineering for Gas Turbines and Power*, Vol. 129, pp. 877–894.

Cifuentes, L., Kempf, A. and Dopazo, C., 2019. "Local entrainment velocity in a premixed turbulent annular jet flame". *Proceedings of the Combustion Institute*, Vol. 37, pp. 2493–2501.

De, S., Agarwal, A.K., Chaudhuri, S. and Sen, S., eds., 2018. *Modeling and Simulation of Turbulent Combustion*. Springer Singapore.

Frenklach, M., Wang, H., Goldenberg, M., Smith, G.P., Golden, D.M., Bowman, C.T., Hanson, R.K., Gardiner, W.C. and Lissianski, V., 1995. "Gri-mech - an optimized detailed chemical reaction mechanism for methane combustion".

Kabanshi, A. and Sandberg, M., 2019. "Entrainment and its implications on microclimate ventilation systems: Scaling the velocity and temperature field of a round free jet". *Indoor Air*, Vol. 29, pp. 331–346.

Launder, B. and Spalding, D., 1974. "The numerical computation of turbulent flows". *Computer Methods in Applied Mechanics and Engineering*, Vol. 3, pp. 269–289.

Magnussen, B., 1981. "On the structure of turbulence and a generalized eddy dissipation concept for chemical reaction in turbulent flow". American Institute of Aeronautics and Astronautics.

Magnussen, B. and Hjertager, B., 1977. "On mathematical modeling of turbulent combustion with special emphasis on soot formation and combustion". *Symposium (International) on Combustion*, Vol. 16, pp. 719–729.

Marchisio, D.L. and Barresi, A.A., 2009. "Investigation of soot formation in turbulent flames with a pseudo-bivariate population balance model". *Chemical Engineering Science*, Vol. 64, pp. 294–303.

Menter, F.R., 1994. "Two-equation eddy-viscosity turbulence models for engineering applications". *AIAA Journal*, Vol. 32, pp. 1598–1605.

Oldenhof, E., Tummers, M.J., van Veen, E.H. and Roekaerts, D.J., 2011. "Role of entrainment in the stabilisation of jet-in-hot-coflow flames". *Combustion and Flame*, Vol. 158, pp. 1553–1563.

Pope, S.B., 2000. *Turbulent Flows*, Vol. 1. Cambridge University Press, 10th edition.

Ricou, F.P. and Spalding, D.B., 1961. "Measurements of entrainment by axisymmetrical turbulent jets". *Journal of Fluid Mechanics*, Vol. 11, pp. 21–32.

Shih, T.H., Liou, W.W., Shabbir, A., Yang, Z. and Zhu, J., 1995. "A new k-epsilon eddy viscosity model for high reynolds number turbulent flows". *Computers & Fluids*, Vol. 24, pp. 227–238. ISSN 00457930.

Tesner, P., Smegiriova, T. and Knorre, V., 1971. "Kinetics of dispersed carbon formation". *Combustion and Flame*, Vol. 17, pp. 253–260.

Turutoglu, C. and Cadirci, S., 2023. "Improvement of standard k-epsilon turbulence model for round free jets by adjusting closure coefficients". American Society of Mechanical Engineers.

Versteeg, H.K. and Malalasekera, W., 2007. *An Introductionto Computational Fluid Dynamics*, Vol. 1. Pearson, 2nd edition.

Widmann, J.F., 2003. "Evaluation of the planck mean absorption coefficients for radiation transport through smoke". *Combustion Science and Technology*, Vol. 175, pp. 2299–2308.

Yang, B., Hu, B. and Koyly, U.O., 2005. "Mean soot volume fractions in turbulent hydrocarbon flames: A comparison of sampling and laser measurements". *Combustion Science and Technology*, Vol. 177, pp. 1603–1626.

7. RESPONSIBILITY NOTICE

The authors are the only responsible for the printed material included in this paper.